Comparison of intense nightside shock-induced precipitation and substorm activity

M. Meurant,[1] J.-C. Gérard,[1] C. Blockx,[1] V. Coumans,[1] B. Hubert,[1] M. Connors,[2] L. R. Lyons,[3] and E. Donovan[4]

Received 24 November 2004; revised 30 March 2005; accepted 19 April 2005; published 28 July 2005.

[1] Sudden variations of the solar wind dynamic pressure frequently induce dayside enhancements of auroral activity with features such as high-latitude arcs, low-latitude proton flashes, and enhancement of auroral precipitation propagating dawnward and duskward from noon to the night sector. In some cases, these shocks also induce enhanced activity during which the power precipitated into the night sector may reach values as high as observed during substorms. Several studies have shown that the triggering of nightside-enhanced precipitation is more likely during periods of southward interplanetary magnetic field (IMF) components. Early works showed that substorm-like activity is not frequent after a shock and suggested that shocks may not be considered as substorm triggers. We examine up to what point substorm-like nightside activity triggered by a shock is comparable to an isolated substorm. For this purpose, we analyze three events morphologically similar to substorms and occurring within less than 20 min after the arrival of a pressure pulse on the front of the magnetosphere. Different features of these events such as the mean energy of precipitated electrons, the latitudinal motion of boundaries before and after onset, and the power precipitated into the nightside sector are compared with isolated substorms. We conclude that the characteristics of shock-induced substorms appear very similar to those of isolated substorms. Shocks are able to trigger substorms when they hit an unstable magnetosphere. The interpretation is that the perturbation due to the shock induces a substorm by closure of the plasma sheet magnetic field. For the events presented in this study, the instability result from a period of southward IMF or stretching of the magnetic tail induced by a previous shock.

Citation: Meurant, M., J.-C. Gérard, C. Blockx, V. Coumans, B. Hubert, M. Connors, L. R. Lyons, and E. Donovan (2005), Comparison of intense nightside shock-induced precipitation and substorm activity, *J. Geophys. Res.*, *110*, A07228, doi:10.1029/2004JA010916.

1. Introduction

[2] Several studies [*Schieldge and Siscoe*, 1970; *Kawasaki et al.*, 1971; *Burch*, 1972; *Kokubun et al.*, 1977; *Akasofu and Chao*, 1980; *Zhou and Tsurutani*, 1999; *Tsurutani et al.*, 2001; *Meurant et al.*, 2004] have established that sudden dynamic pressure (P_{dyn}) variations (also called shocks or sudden impulses) frequently induce enhanced dayside auroral emissions. Generally, emissions induced by shocks appear at high latitudes (between 60° and 75° geomagnetic latitude (MLAT)). The typical development of a shock-induced aurora begins as an enhanced activity in the noon sector. Within a few minutes, the region of auroral intensification expands longitudinally at speeds of 6 to 11 km s^{-1}, reaching the dawn and dusk sectors and eventually filling most of the nightside oval. *Liou et al.* [1998] and *Boudouridis et al.* [2003] have highlighted the effects on the precipitated power of a period of southward B_z preceding the shock. *Meurant et al.* [2004] described the role of solar wind (SW) speed, the magnitude of the interplanetary magnetic field (IMF), and the orientation of B_z carried with the shock on the induced precipitated power. Another type of dayside auroral emission generated by the perturbation of the magnetosphere by shocks was described by *Hubert et al.* [2003, 2004]. They observed low-latitude emissions (~60°) in the noon sector due to protons, occurring within a short time period (typically 5 min) following the arrival of the shock on the front of the magnetosphere.

[3] Nightside shock-enhanced activity may result either from an expansion of dayside precipitation, from an initiation starting in the night sector or from a superposition of these two effects. *Zhou and Tsurutani* [2001] have classified nightside activity into three categories, depending of the intensity of the activity enhancement: quiescent event, pseudobreakups, and substorms. They highlight a correlation between the orientation of B_z during the 90 min preceding the shock and the intensity of the nightside enhancement. They characterize a substorm as a "sudden

[1]Université de Liége, Liége, Belgium.
[2]Athabasca University, Athabasca, Alberta, Canada.
[3]University of California, Los Angeles, California, USA.
[4]University of Calgary, Calgary, Alberta, Canada.

0148-0227/05/2004JA010916$09.00

auroral illumination increase'' and they illustrate it by the enhancement of a preexisting activity. As *Kokubun et al.* [1977], they found that 43% of the shocks induce magnetic bays which are frequently associated with substorms. In fact, the ability of a shock to enhance preexisting auroral activity and its eventual ability to trigger an isolated substorm may be viewed as two different questions.

[4] In contrast to these results suggesting that shocks are able to trigger substorms, *Liou et al.* [2003] have shown that magnetic bays induced by a shock are only rarely associated with auroral breakups (18%) and they concluded that shock compressions are not likely to trigger substorms. *Chua et al.* [2001] and *Boudouridis et al.* [2003] distinguish the auroral response initiated by a shock in the nightside region and substorm responses. They argue that substorm enhancements are much more localized than those observed a short time after the arrival of a shock. *Chua et al.* [2001] also point out that the broad emission observed in the nightside after a shock is diffuse, whereas the typical enhancement observed during substorms occurs along discrete arcs which are associated with field-aligned currents. In their conclusion, *Boudouridis et al.* [2003] raise the question under what condition, if any, substorm triggering might take place during sudden enhancement of the solar wind dynamic pressure. They suggest the possibility of such a succession of events but do not provide observations to support this.

[5] This study addresses the question of the ability of a shock to trigger nightside activity presenting the same characteristics as substorms or its ability to trigger only nightside activity which may be intense and/or global, but which is fundamentally different from substorms. Case studies used to investigate this question are selected based on several criteria. They occur within a short time after the arrival of the shock (<20 min), they start as an intense and localized increase of precipitation in the midnight sector similarly to substorm expansive phase onset (to avoid confusion with different types of intense nightside events) and they are preceded by a period of weak activity compared to the level observed after the shock. We define a shock as an increase of the dynamic pressure by a factor of 1.6 in less than 15 min, which is a relaxed definition compared with our previous study [*Meurant et al.*, 2004]. Different characteristics of these events are presented to allow a comparison with isolated substorms. Earlier works [*Lyons et al.*, 1997; *Liou et al.*, 2003; *Hsu and McPherron*, 2004] already linked triggering of substorms with processes internal to the magnetosphere or with variations of IMF such as a B_z turning. On the basis of a case study, *Brittnacher et al.* [2000] also investigated the role of the IMF and the dynamic pressure variation on the triggering of a substorm. Similarly, this work addresses the question of the role of solar wind parameters and dynamic pressure (P_{dyn}) jumps as substorm initiators.

[6] A second question addressed in this study is up to what point similarities and differences between isolated substorms and shock-induced substorms provide information on physical processes responsible for substorms. This discussion is based on the time delay between the onset and the arrival of the shock on the magnetosphere and on the elevation angle of magnetic field lines for shock-induced substorms in comparison to isolated substorms. The time delay between the arrival of the shock and the onset observation is calculated by comparing the Advanced Composition Explorer (ACE) solar wind data propagated to the magnetopause with the time of the auroral onset. The elevation angle of magnetic field lines is measured at geosynchronous orbit by Geostationary Orbiting Environmental Satellite (GOES) satellites.

[7] Data used for this study are obtained by spacecraft as well as ground-based instruments. The WIC and SI12 cameras in the FUV instrument of the IMAGE satellite [*Burch*, 2000] provide snapshots of the auroral region with a 2-min time resolution. The WIC camera is mostly sensitive to emissions excited by electron precipitation. The passband (between 140 and 180 nm) includes the LBH bands and the NI 149.3 nm line. Excitation of the LBH bands and the NI lines is produced by incident primary electrons, protons, and secondary electrons colliding with N_2 molecules. WIC images have 256 $\times$ 256 pixels subtending a 70 $\times$ 70 km^2 square from apogee. The SI12 imager approximately covers the same field of view as the WIC camera, with 128 $\times$ 128 pixels. It is sensitive to the Doppler-shifted Lyman-α auroral emission. As precipitating protons collide with neutral atmospheric constituents, they can capture an electron and temporarily become fast hydrogen atoms. A fraction of the fast H atoms are produced in the H(2p) state and radiate Doppler-shifted Lyman-α photons [*Mende et al.*, 2001; *Gérard et al.*, 2001]. Quantitative information on the electron mean energy, electron energy flux, and proton energy flux can be deduced from FUV data. Uncertainties of this method were extensively discussed by *Meurant et al.* [2003a] and *Coumans et al.* [2004]. These quantities may be deduced since FUV includes three imagers, with two of them (WIC and SI13) mostly sensitive to the electron aurora and the third (SI12) exclusively responding to proton precipitation. Quantitative information deduced from FUV images may be altered by airglow and reflected sunlight contamination of WIC and SI13 data. This difficulty is usually adequately solved by a subtraction method based on the model proposed by *Immel et al.* [2000]. However, this correction was not considered in this study since the regions of interest are located in the 1800–0600 MLT sector, which is entirely in darkness during the periods of the year considered here. GOES 8 and 10 spacecraft are used to determine the magnetic field line configuration and its departure from a dipolar topology. GOES 8 and 10 are geosynchronous satellites crossing the midnight sector respectively around 0500 UT and 0945 UT. Solar wind (SW) and interplanetary magnetic field (IMF) conditions prevailing before and during studied events were obtained by the ACE satellite located at $\sim$1.4 $\times$ 10^6 km sunward from the Earth and by GEOTAIL. ACE data are propagated to the magnetopause as described by *Weimer et al.* [2003]. Ground-based magnetometers from IMAGE and CANOPUS networks are also used as well as Meridian Scanning Photometers based at Gillam, Canada.

[8] Section 2 is dedicated to the description of characteristics of typical isolated substorms observed with IMAGE-FUV. Section 3 presents observations of shock-triggered substorms and provides a detailed description of the four events selected for the comparison. Finally, results are

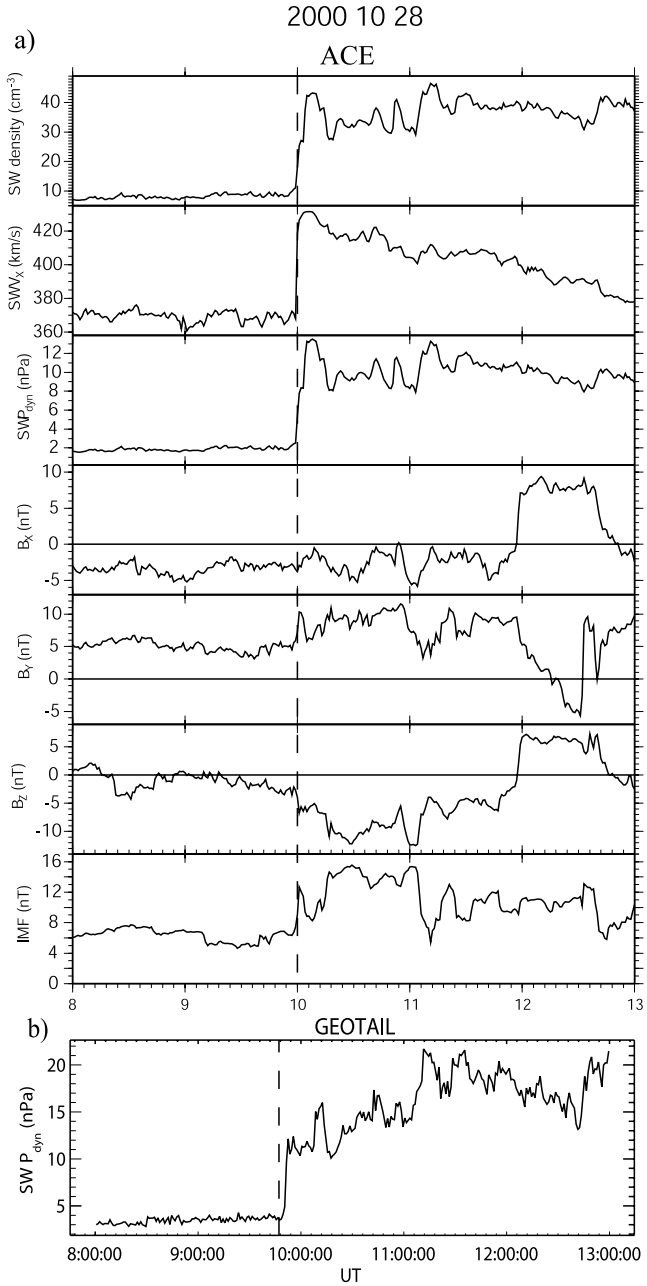

Figure 1. (a) Solar wind (SW) and interplanetary magnetic field (IMF) data recorded by the ACE satellite the 28 October 2000 and propagated to the magnetopause. The time of the shock is indicated by the vertical dashed line. (b) Dynamic pressure recorded by the GEOTAIL satellite during the same period.

discussed in section 4 and conclusions are presented in section 5.

2. Typical Observations During Isolated Substorms

[9] To facilitate the comparison with events described in this paper, we first briefly summarize the typical behavior of substorms as observed with IMAGE-FUV and GOES. In their study of the statistical behavior of proton and electron precipitation during substorms based on 91 cases, *Mende et al.* [2003] reported that prior to onset, an equatorward motion of the mean low-latitude boundary of the electron and proton aurora is observed, but they found no evidence of intensity fading in their statistic. This equatorward motion is seen on the statistical behavior but is not observed for each individual event. *Gérard et al.* [2004] observed a spatial and temporal coincidence of the onsets of electron and proton aurora within the 2-min resolution of FUV. After onset, both electron and proton auroras expand largely poleward and moderately equatorward. The poleward expansion is faster and more pronounced for electrons than for protons and the intensity enhancement at onset is also more significant for electrons. The times of the peak of the energy dissipation and the recovery times often differ for electron and proton. *Hubert et al.* [2003] determined values of the power precipitated in the nightside varying from 20 GW to over 100 GW. They also note that the fractional power of proton precipitation decreases when the global activity increases. They found proton relative contributions between 10 and 20% during active periods. If these values are scales by a factor of 0.5 as suggested by *Coumans et al.* [2002], a relative proton contribution of 5–10% is obtained for high activity periods. The evolution of the configuration of magnetic field lines threading the onset sector may also be considered as a signature of the substorm process. During the growth phase (prior to the onset), the magnetic field at geosynchronous orbit becomes stressed [*Fairfield and Ness*, 1970; *Sauvaud and Winckler*, 1980; *Kokubun and McPherron*, 1981; *Nagai*, 1982; *Kaufmann*, 1987; *Lopez et al.*, 1998], corresponding to an increased cross-tail current. The corresponding stretching is abruptly stopped at substorm onset as the configuration changes from a tail-like to a dipole-like configuration [*Cumming et al.*, 1968; *McPherron et al.*, 1973; *Sauvaud and Winckler*, 1980; *Kokubun and McPherron*, 1981]. This dipolarization is interpreted as a diversion of the cross-tail current into the ionosphere [*Bonnevier and Rostoker*, 1970; *McPherron et al.*, 1973; *Rostoker*, 1974]. The dipolarization starts in a longitudinally confined region and is followed by an azimuthal expansion after onset [*Kokubun and McPherron*, 1981; *Nagai*, 1982]. Using GOES 8 and 9 and POLAR-VIS data, *Liou et al.* [2002] presented a superposed epoch analysis of 32 substorm events. They confirmed that continuous stretching of magnetic field lines is a typical preonset signature. For moderate to large substorms, the stretching process typically lasts 1 hour. They also show that after onset, the average field configuration returns at a faster speed to its presubstorm level in ~10 min. They note that an overcompression of the dipolarized magnetic field can occur ~10 min after the onset and may last over 1 hour. The period of reconfiguration from a tail-like to a more dipole-like orientation coincides with the substorm expansion phase.

3. Data

3.1. Event of 28 October 2000

[10] The shock triggering this event corresponds to an increase of the dynamical pressure (P_{dyn}) measured by the ACE satellite from 2.5 nPa to 13 nPa in 6 min which starts a few minutes before 1000 UT (Figure 1a) and is associated

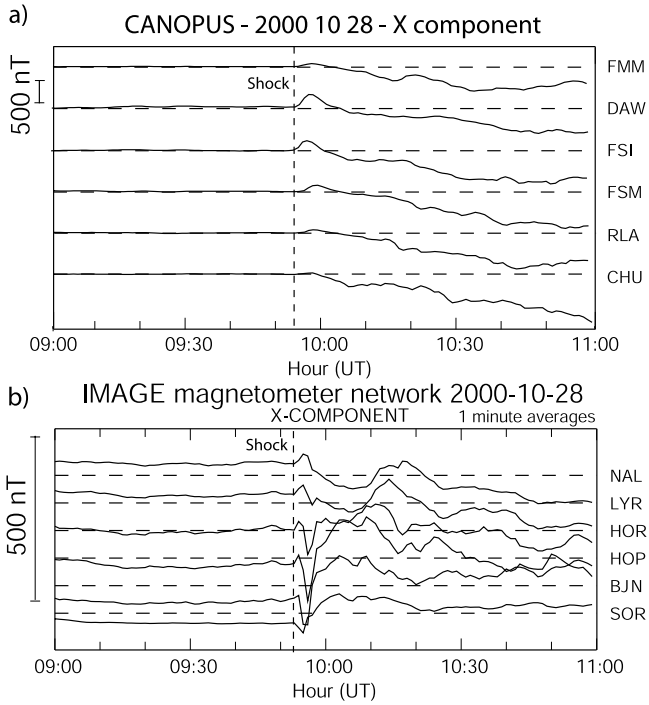

Figure 2. (a) Traces of ground magnetic perturbations from 0900 to 1400 UT on 28 October 2000, as observed at CANOPUS stations. Except for the top trace, stations are located at 68° magnetic north and are arranged from west to east proceeding from the bottom. The top panel is from Ft. McMurray, at roughly 65° magnetic latitude. From bottom to top, the other panels show Dawson, Fort Simpson, Fort Smith, Rabbit Lake, and Churchill. In each panel the X component is shown. A quiescent period precedes the shock arrival at 0955 UT. An initial rise in X at that time is generally attributed to compression and is strongest in the morning sector (Churchill). A disturbed period follows as described in the text. (b) Traces of the X component of the magnetic perturbation from 0900 to 1100 UT, as observed by the IMAGE magnetometer network between 67° and 76° MLAT. Coordinates of the stations may be found at http://www.ava.fmi.fi/image/coordinates.html.

with an increase of the IMF intensity during a period of southward B_z. The GEOTAIL satellite was located in the dawn sector during this event (X = 12.6; Y = 26.3; Z = 0.45 R_E), outside the magnetosphere and observed an enhancement of the P_{dyn} at 1006 UT, i.e., more than 6 min after the main enhancement and less than 2 min before the nightside onset observed at 1008 UT (Figure 1b). Since the IMAGE-FUV field of view only intercepted the onset region ~8 min after the arrival of the pressure pulse, we use ground-based data before 1008 UT. The Kp value was 3 during the 3 hours preceding the shock, 5 during the event, and 4 during the next 3 hours. Owing to the lack of FUV data before the arrival of the shock, it cannot be determined whether a growth phase developed before the arrival of the shock. However, no evidence of growth phase (stretching of the magnetic field and equatorward motion of the oval) is visible on Figures 2, 3, and 5. Magnetograms plotted on Figure 2a are obtained from the ground by CANOPUS stations located in the postmidnight sector (0100–0500 MLT) when the shock hit the magnetosphere and Figure 2b displays the x-component of magnetograms recorded by the IMAGE network in the prenoon region (10.8–11.6 MLT). The perturbation observed on these magnetograms coincides with the shock arrival time (observed by IMAGE 1 min before CANOPUS) and do not present signature of growth phase before this time. Keograms presented in Figure 3 were obtained by Meridian Scanning Photometers (MSP) at the Gillam station (located at 0400 MLT, MLAT = 67°, MLON = −29°). Emissions due to proton and electron precipitations both present a clear enhancement of activity at ~0956 UT following a period of low activity. Before the enhancement, no equatorward motion of the oval boundaries is observed. Such an equatorward motion is statistically considered as a substorm signature but it is not systematically observed on all substorm events [*Mende et al.*, 2003]. As seen in Figure 4, the intensification of nightside activity is observed with WIC and SI 12 around 2330 MLT at 1008 UT. Subsequent nightside activity is characterized by westward and eastward propagation (Figure 4). The motion of the poleward boundary is significant, whereas there is only a small shift of the equatorward boundary (Figures 3 and 4). In the onset region, the intensity reaches its maximum value around 10 min after the onset of the nightside aurora (not shown).

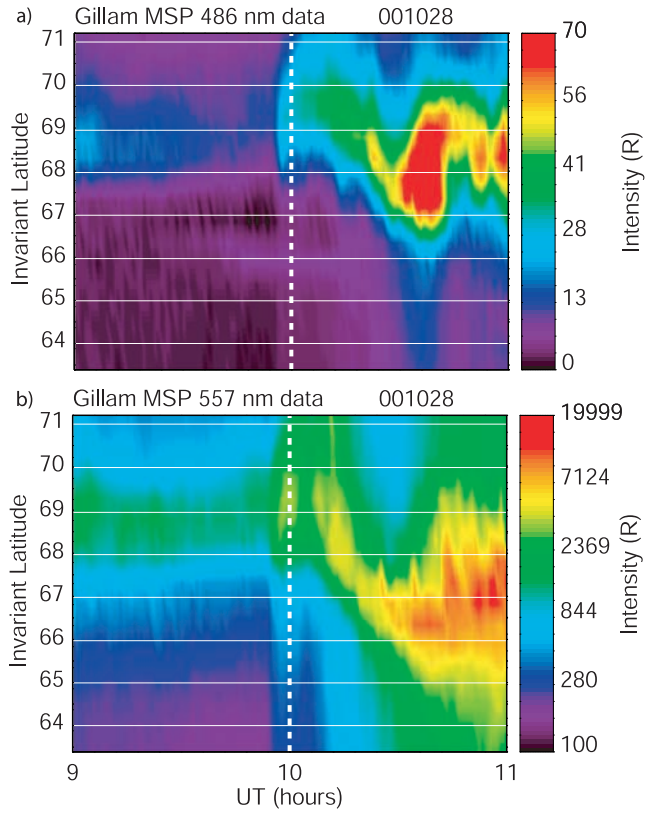

Figure 3. Keogram representing the evolution of brightness along the time observed by Meridian Scanning Photometers at the the Gillam station (located at MLAT = 67°, MLON = −29°). Emissions due to (a) protons (λ = 486 nm) and (b) electrons (λ = 557 nm) precipitations are presented.

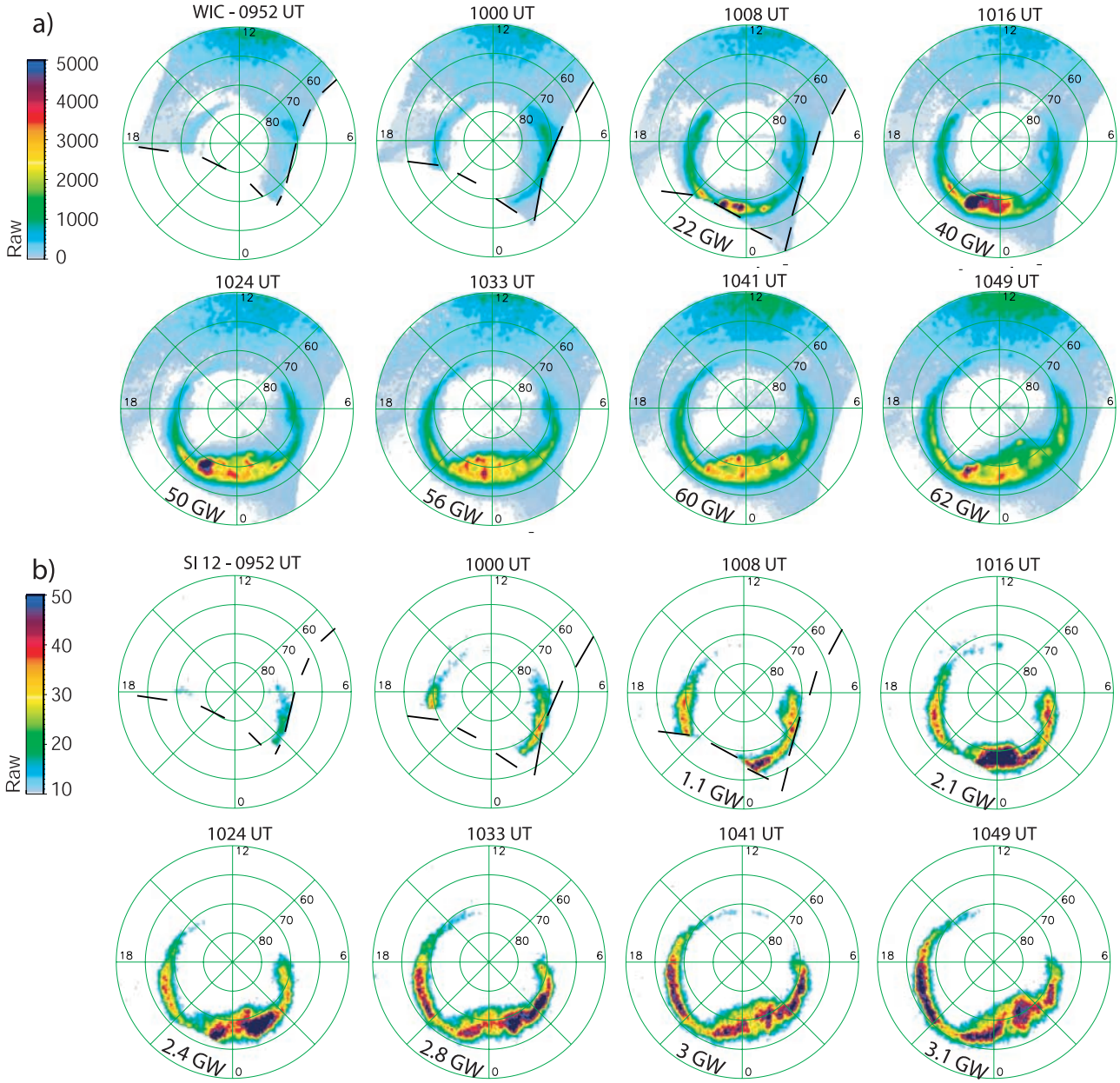

Figure 4. Sequence of WIC (top) and SI12 (bottom) images of the northern hemisphere displayed on a geomagnetic grid with local noon at the top of each image. The data were obtained on 28 October 2000 between 0952 and 1049 UT. The WIC signal is mainly due to electron precipitation and the SI12 instrument is solely sensitive to proton aurora. Dashed lines drawn on the first three images represent the field of view of the instrument at these times. Power precipitated in the night region is indicate at the bottom of each panel. The magnetic local time of MSP, CANOPUS, IMAGE network, GOES 8 and GOES 10 are 0400, 0100–0500, 1050–1135, 0500, 0030 MLT, respectively.

During the next 50 min, the total power injected into the night sector continues to grow, reaching a maximum of ~60 GW (not shown). An atypical parallel increase of the relative proton contribution with the global activity in the observation region is also observed (not shown). A maximum relative proton contribution of 5–6% is observed, what is usual during substorms [*Coumans et al.*, 2002; *Hubert et al.*, 2002]. The mean electron energy precipitated in a 2 MLT sector surrounding the onset location between 60° and 80° MLAT is ~10 keV. It reaches values higher than 17 keV in a region located at the same local time as the onset but 5° MLAT higher (22.6–22.8 MLT, 70°–74° MLAT). The variation of the stretching of magnetic field lines (measured by the elevation angle) observed by GOES 8 and GOES 10 satellites is displayed in Figure 5. When the shock reaches the magnetosphere, these two spacecraft are located in the postmidnight region (~0030 MLT for GOES 10 and ~0500 MLT for GOES 8). The magnetic field is slightly more stretched from a dipolar configuration during hours preceding the shock and no stretching is taking place.

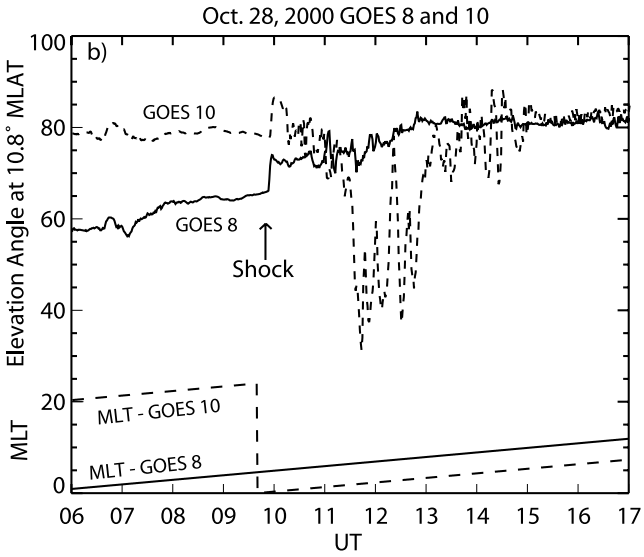

Figure 5. Time evolution of the elevation angle deduced from GOES 8 (solid) and GOES 10 (dashed) data during the 28 October 2000 event between 0600 and 1700 UT. The MLT position of spacecrafts is plotted at the bottom of each panel.

A sudden compression of 9.5° at local midnight and 8.5° at 0400 MLT occurs at the arrival time of the shock. Probably because of the long period of enhanced P_{dyn}, GOES 10 observes an important stretching of the magnetic field during hours after the shock, which was not observed by GOES 8 a few hours before. This stretching appears consequently as a temporal variation probably due to the arrival of the shock. Note also that the angles measured by GOES 8 and 10 are not comparable since these two spacecraft are located at different magnetic latitudes.

3.2. Event of 28 November 2000

[11] An increase of P_{dyn} from 5 nPa to 9 nPa was measured by the ACE satellite and reached the magnetopause at ~1245 UT (Figure 6). A moderate B_z turning which could eventually influence on the evolution of the nightside activity is observed after the shock. Figure 7 represents the time evolution of the elevation angle deduced from GOES data for this event. As plotted in the bottom of Figure 7, GOES 8 and 10 were located at 0746 MLT and 0307 MLT when the shock hit the magnetosphere. During the hour preceding the shock, GOES 10 observed a signature of growth phase by the stretching of magnetic field lines, indicating a loading of the magnetosphere during this period. This stretching is not observed (or significantly weaker) by GOES 8 due to its location in the morning sector. Magnetometers from the CANOPUS network also suggest that a growth phase started before the arrival of the shock (not shown). Figure 8 shows the first nightside enhancement at 1249 UT, about 4 min after the calculated arrival time. As for the previous event, the effect of the shock is observed by GOES 8 and 10 as a compression of the magnetic field lines. At ~0300 MLT (GOES 10), this compression occurs during a period of stretching magnetic field, which probably explains the short time delay between the shock and the onset of activity. After the onset, activity

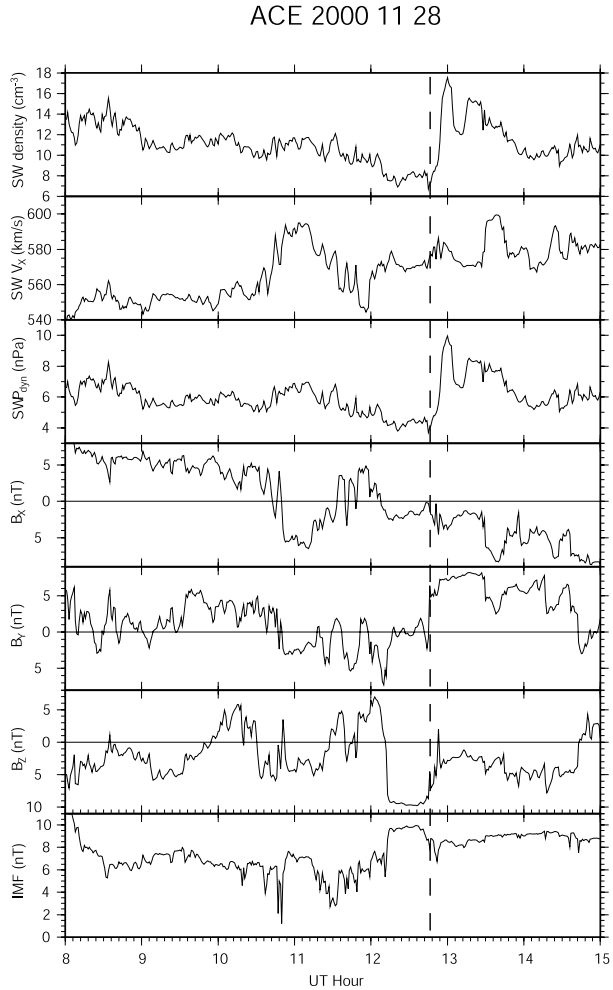

Figure 6. Same as Figure 1a for the 28 November 2000 event.

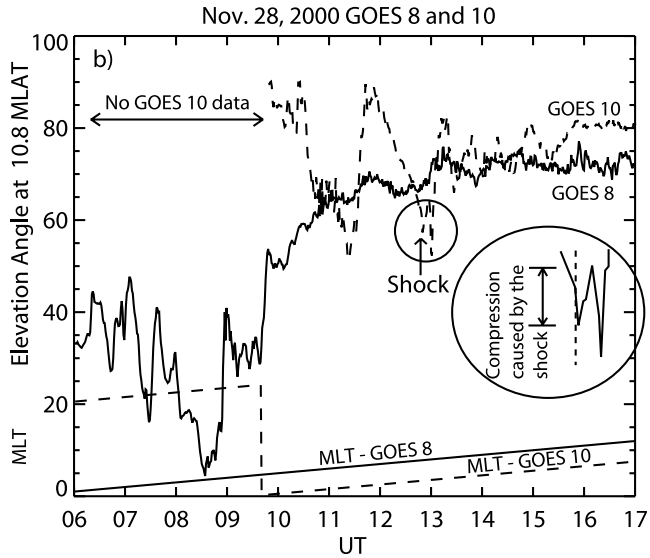

Figure 7. Same as Figure 5 for the 28 November 2000 event.

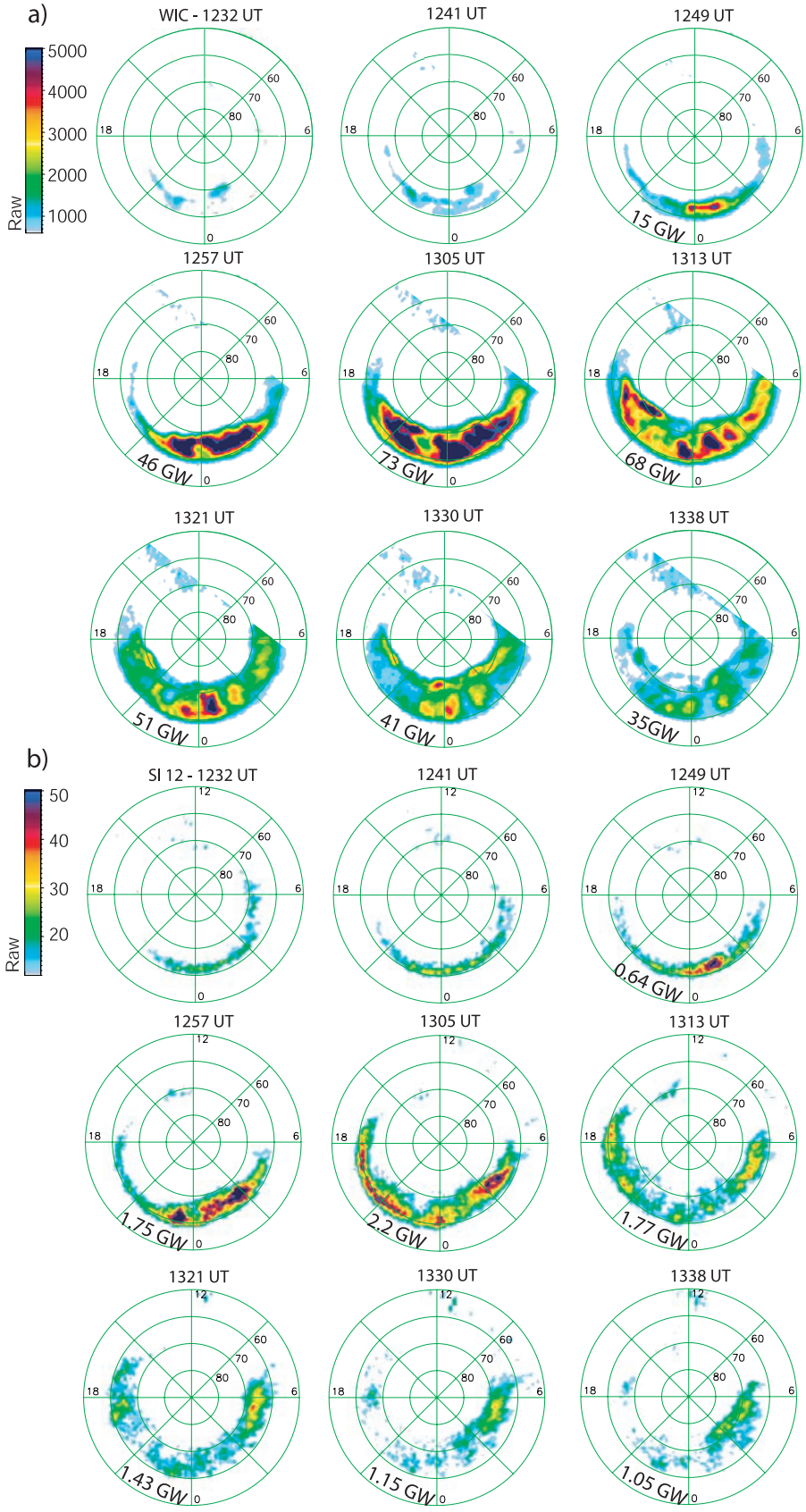

Figure 8. Same as Figure 4 for the 28 November 2000 event. The magnetic local time of MSP, CANOPUS, IMAGE network, GOES 8 and GOES 10 are 0700, 0400–0800, 1400–1500, 0746, 0307 MLT, respectively.

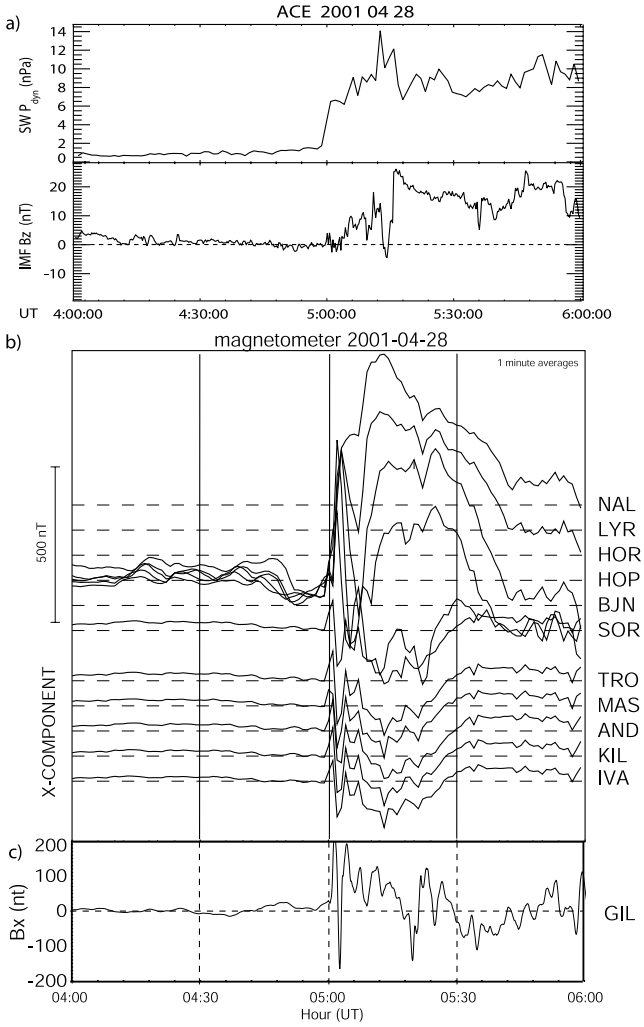

Figure 9. (a) Time evolution of the dynamic pressure and the B_z component during the 28 April 2001 event. These data are recorded by ACE and shifted by the travelling time of the shock between ACE and the front of the magnetosphere. (b) Same as Figure 2b for the 28 April 2001 event. (c) Same as Figure 2a at Gillam station for the 28 April 2001 event.

propagated eastward and westward, finally filling the entire nightside sector at auroral latitudes after 13 min. As shown in Figure 8, no motion of equatorward boundaries of the electron or proton precipitation can be observed during 30 min after onset. The poleward electron and proton boundaries move poleward during these 30 min. During the first 10 min following the onset, the additional power injection in the entire night sector reaches ~70 GW (not shown). A decrease of the proton relative contribution is observed when the global activity increases (3% during the expansive phase of the substorm). The electron mean energy and electron energy flux in the onset area deduced from FUV exceed the 20 keV and 15 mW/m^2 which are the limits of the method [*Meurant et al.*, 2003a]. A second enhancement of P_{dyn} is observed 30 min after the first one. A dipolarization of the tail magnetic field associated with this second pulse is observed by GOES 10. However, no induced activity is observed by FUV, probably due to the high level of auroral activity at this time.

3.3. Event of 28 April 2001

[12] The dayside activity of this event and its propagation to the nightside region were extensively described by *Meurant et al.* [2003b]. This event occurred following a long period of $B_z \sim 0$ nT. The shock was characterized by an increase of P_{dyn} from 1 to 10 nPa in 10 min and reached the magnetopause at 0458 UT (Figure 9).

[13] Before the onset, activity propagated from the day to the night sector but the midnight region remained unaffected by the surge. The propagation of the dayside activity to the night region was followed by an onset in the midnight sector 21 min after the first shock-induced dayside enhancement. A second enhancement of P_{dyn} and simultaneous variations of B_z (with a short excursion to negative values) are observed a few minutes before onset (Figure 9a). After the onset, the evolution of the enhancement of activity on the nightside is different from events presented before as no eastward and westward propagation of activity is observed. During this enhancement illustrated in Figure 10, the onset evolves into a transpolar structure stretching from the oval to the inside of the polar cap in the midnight region.

[14] On the basis of the speed of propagation from dayside along the oval, it was suggested that the enhancement along the oval is due to the perturbation of the near-Earth magnetic field. This propagation speed corresponds to the travel of the shock along the magnetosphere [*Zhou and Tsurutani*, 1999]. According to this view, the midnight sector may stay inactive since magnetic field lines threading this region are stretched down the tail. Because of this stretching, field lines cross the plasma sheet at large distances from the Earth and a longer time is needed for the magnetospheric perturbation to affect these lines. The description of the propagation of the perturbation along the near Earth field lines can be completed by observations of the magnetic field in the midnight region shortly after the shock.

[15] Magnetograms recorded by the IMAGE network (located in the morning sector during this event) show the arrival of the perturbation at 0458 UT (Figure 9b) on a wide range of magnetic latitudes (65°–75°). The same perturbation is observed 2 min later in the premidnight region by magnetometers (Figure 9c) and MSP (not shown) at the Gillam station. MSP data shows a very low activity before the arrival of the shock, a rapid widening of the active region after the shock and an important intensification at ~0520 UT. This sequence of events is in fairly good synchronism with the sequence of FUV images in Figure 10. The intensification and the widening of the active region observed by Gillam's MSP is due to the propagation of activity from the day to the night region and the important intensification corresponds to the onset observed around the local midnight at 0521 UT. ACE and GEOTAIL data indicate that this intensification in the midnight sector follows a second increase of the dynamic pressure and a strong intensification of the northward B_z component (Figure 9a). After onset, the activity propagates into the night sector and along a transpolar axis (Figure 10). The power precipitated in the entire night region reaches its maximum after 0520 UT and is characterized by an unusu-

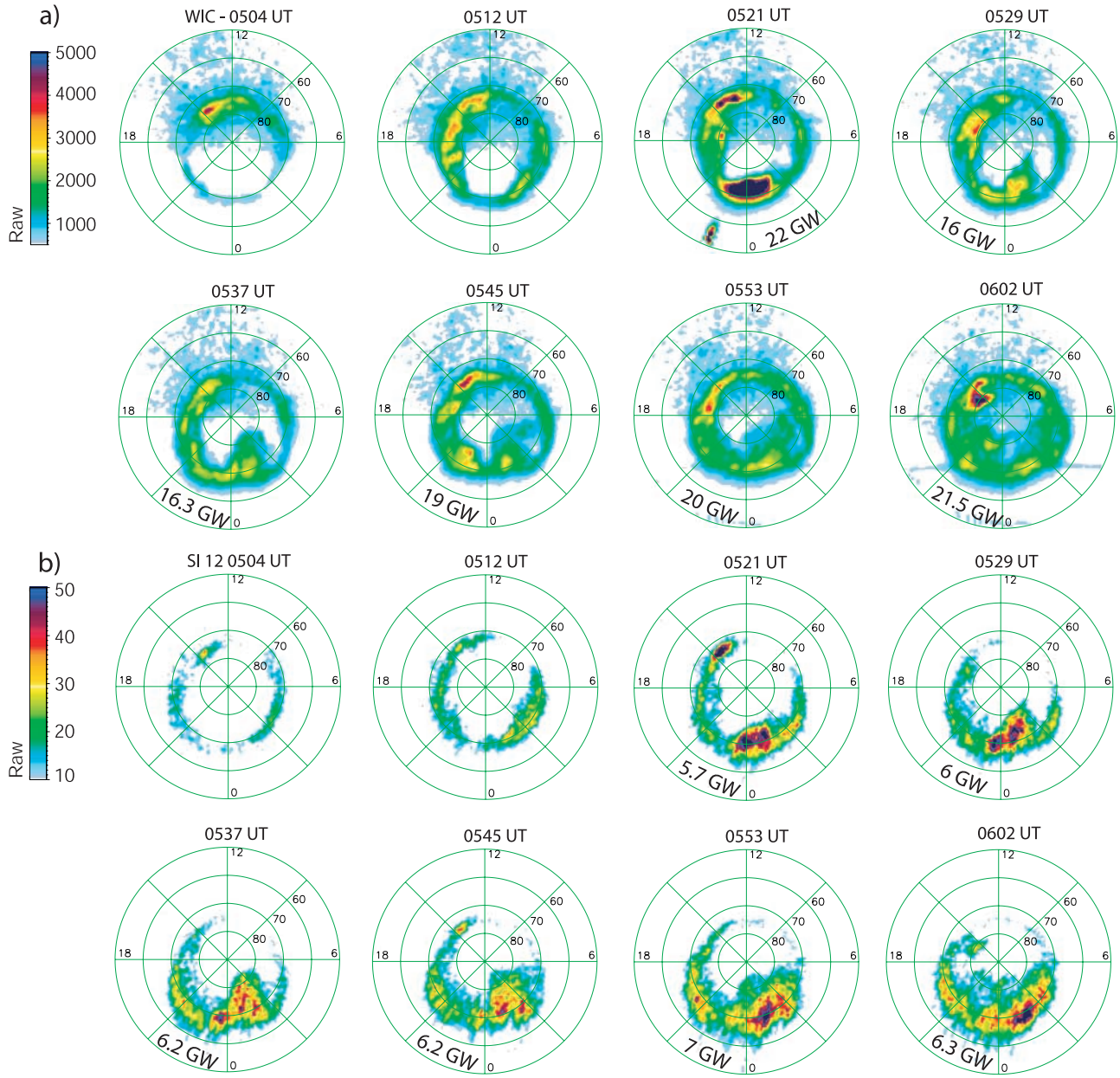

Figure 10. Same as Figure 4 for the 28 April 2001 event. The magnetic local time of MSP, CANOPUS, IMAGE network, GOES 8 and GOES 10 are 2300, 2000–0100, 0600–0700, 0000, 1930 MLT, respectively.

ally large contribution of proton precipitation of 20% (not shown).

[16] The perturbations of the tail magnetic field induced by these SW and IMF perturbations were observed by the GOES 8 and 10 satellites (Figure 11). Elevation angles plotted at Figure 11b are obtained in the 23.7 MLT to 0.7 MLT region and represent a proxy of the field line stretching. A close time coincidence is observed between the shock arrival at 0458 UT and the beginning of the decrease of elevation angle. After the shock, simultaneously to the tail magnetic field line stretching, dayside activity appears and propagates into the night region but no electron or proton auroral activity is observed in the midnight sector. According to the propagation model of the perturbation described before, precipitation observed during this period is probably due to the perturbation of near-Earth field lines. At ~0521 UT, a short-time compression of tail field lines is observed probably caused by the conjugate effects of the second increase of dynamic pressure and a decrease of clock angle (Figure 9a). Subsequent to this compression, electron and proton precipitation similar to a substorm expansive phase onset is observed by FUV. FUV data obtained when the elevation angle was identical during the stretching phase (0515 UT) shows that only weak precipitation was then observed in the midnight region. The large amount of precipitation observed at 0521 UT is thus clearly linked to the dynamics of field lines rather than to a static configuration of the magnetosphere. Figure 11a show the variation

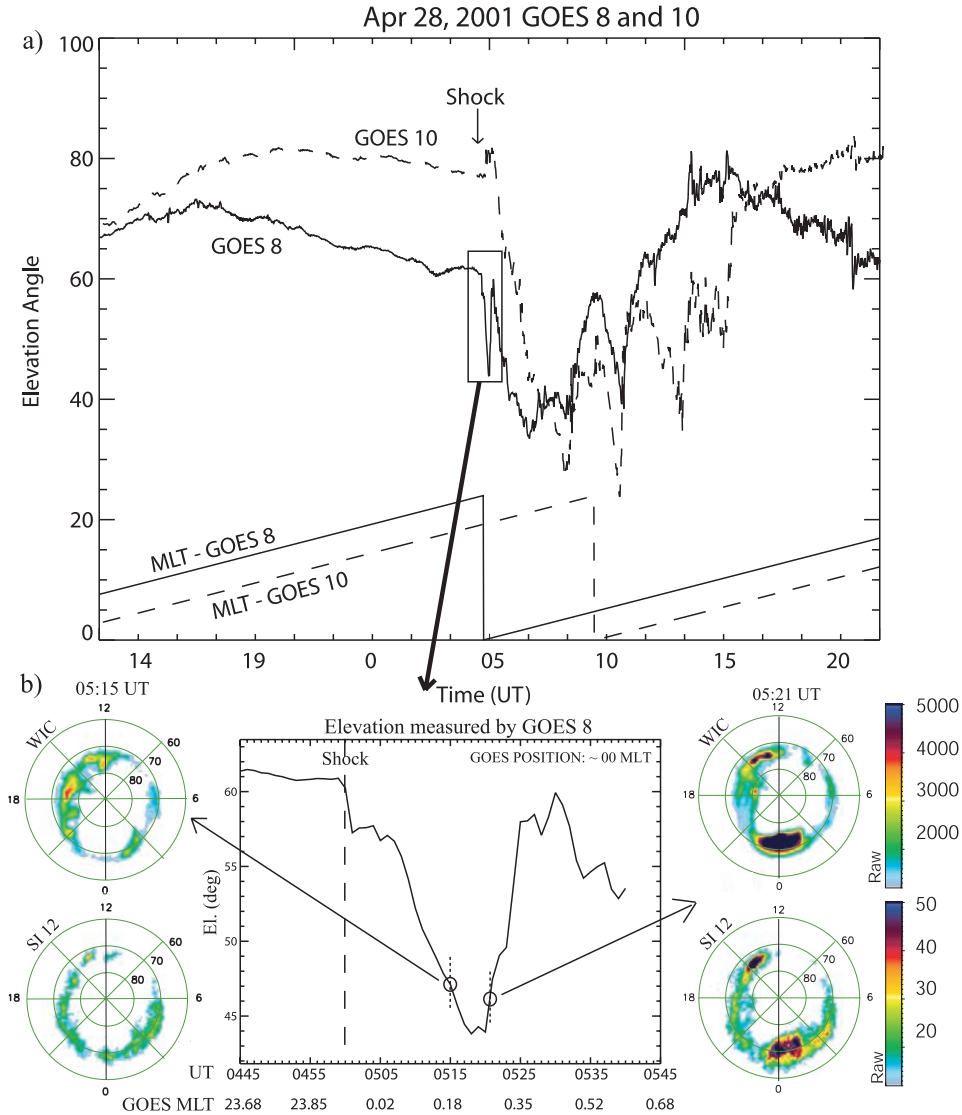

Figure 11. (a) Same as Figure 5 for the 28 April 2001 event. (b) Elevation angle of the magnetic field lines measured by GOES 8 in the midnight region during the 28 April 2001 event. The shock is represented by the vertical dashed line. WIC and SI12 data are shown before the minimum of the elevation angle (to the left and bottom) and after this minimum (to the right).

of the elevation angle during a large period around the shock. The compression described before took place during a large stretching observed simultaneously by GOES 8 and 10 in the postmidnight region (0000–0400 MLT) and around midnight (2000–0400 MLT), respectively. During minutes following the arrival of the shock, GOES 10 observed a short-time compression before the beginning of the stretching phase. As suggested for the 28 October 2000 event, this long-time period of tail stretching is probably due to the long period of P_{dyn} enhancement and the induced viscous interaction.

[17] *Liou et al.* [2002] presented the mean evolution of magnetic field lines before and after a substorm expansive phase onset. The sequence starts with a decrease of the elevation angle during the hour preceding the onset (corresponding to the growth phase) and a relaxation during the following 15 min. They also observed a clear relationship between the minimum elevation angle and the timing (observed with POLAR-UVI) of the substorm onset. The behavior described by *Liou et al.* [2002] for substorms is thus remarkably similar to that induced by the shock in the midnight region during this event. We note however that our observations of the time length of the stretching and the relaxation phases are different from the average value reported by *Liou et al.* [2002]. The drop of the elevation angle lasts ~17 min in this case (versus 1 hour for isolated substorms) and the relaxation lasts ~7 min (versus 15 min). The initial configuration of the magnetosphere is more dipolar when the shock arrives (with an elevation of 61°) than values reported by *Liou et al.* [2002] during minutes preceding the growth phase (49°). On the basis of these observations, it is reasonable to believe that a shock may induce the same type of magnetic field line motions as those occurring during isolated substorms and that this magnetic field line dynamics may be considered as the cause of the onset. However, during this event, the observed activity is

probably a pseudobreakup rather than a substorm because of the absence of eastward and westward propagation. The different timing of our observations compared with the *Liou et al.* [2002] results is probably not an indication of a significant difference in the physical process. *Liou et al.*'s [2002] results describe statistical behavior and were built on a sample of 32 events, including events characterized by a shorter characteristic time than the average value.

4. Discussion

[18] A solar wind shock impinging on the magnetosphere appears to induce different types of precipitation. Dayside and nightside activity correspond to different mechanisms. Using the POLAR-UVI imager, *Chua et al.* [2001] have shown that shock pressure pulses arriving on the front of the magnetosphere may induce auroral intensifications presenting different characteristics from isolated substorms. They observed simultaneous brightening over broad areas of the dayside and nightside aurora, indicating that more magnetospheric regions participate as sources for auroral precipitations than during isolated substorms. They also observed a lower mean energy (=7 keV) of electrons precipitated during shock induced events than during isolated substorms (>10 keV). A rapid global nightside enhancement described as a propagation of activity from the noon to the night sector different from a substorm was also observed by *Meurant et al.* [2004]. This propagation is due to the perturbation of field lines crossing the equatorial plane at relatively short distances from the Earth. A review of shock-induced mechanisms was presented by *Zhou et al.* [2003]. In the present study, we describe events with nightside shock-induced activities presenting similarities with substorms. The question addressed here is to determine up to what point some auroral activity triggered by shock in the night sector may be considered as real substorms, that is whether if a shock is able to trigger precipitation mechanisms which induce similar observations to those existing during substorms.

4.1. Comparison Between Shock-Induced and Isolated Substorms

[19] The first two events described in section 3 occurred during periods of southward B_z and show westward and eastward propagation of the activity following initial precipitation in the midnight region. A poleward motion of the poleward boundary is observed after the onset. This expansion and broadening of the precipitation region are similar to a substorm expansive phase. Quantitative characteristics of these two events are also similar to those observed during substorms. The mean energy of precipitated electrons is above 10 keV, the relative contribution of protons to the total precipitated power is ~5% and the precipitated power in the nightside region is comparable to those observed during substorms [*Hubert et al.*, 2002]. No signature of growth phase is observed during the 28 October 2000 event. However, during the 28 November 2000 event, GOES 10 indicates that stretching of the tail magnetic field was occurring when the shock hit the magnetosphere similarly to the stretching observed by *Liou et al.* [2002] for substorms. The existence of this growth phase is confirmed by the boundary motion derived from optical data (not shown).

[20] The third event (28 April 2001) occurred following a long period of B_z close to zero. After the arrival of the shock, the B_z component took on positive values. Even in these conditions, an onset is induced in the midnight sector ~20 min after the main shock reaching the magnetopause and ~8 min after a second enhancement of P_{dyn}. Only after the onset was the evolution of the precipitation different from that occurring for southward B_z. Similarities between shock-induced and isolated substorms deduced from remote sensing data are confirmed by in situ measurements of the dynamics of the magnetic field lines. The typical behavior of the magnetic field before and during a substorm reported by *Liou et al.* [2002] appears similar to that reported in Figure 11b, suggesting that the mechanism triggering substorm expansive phase onsets after a shock is the same as for isolated substorm. The growth phase was likely triggered by the arrival of the main shock. The compression triggering the onset is due to a second enhancement of the P_{dyn}. The relative contribution of precipitated protons is higher than during isolated substorms and the power injected in the nightside is low.

4.2. Timing and Model

[21] The time delay between the arrival of the shock on the magnetosphere and the initial dayside enhancement varies from a few minutes to ~20 min. Using a propagation speed of the perturbation inside the magnetosphere of $\simeq$200 km s^{-1} [*Kozlovsky et al.*, 2005] and a typical earthward velocity of the flow from the tail of 100 km s^{-1} to 400 km s^{-1}, the region where the substorm is initiated is located at distances of 5 to 10 R_E for negative B_z and 12.5 to 19 R_E for the slightly positive event. These values are close to distances generally accepted for isolated substorm initiation, as expected from the similarity between shock-induced substorms and isolated substorms.

[22] Since shock-induced events present many similarities with isolated substorms, we now compare our observations to current substorm models. The timing of events and the amount of stretching of the magnetic field described in section are poorly consistent with the near-Earth neutral line model for substorms [*Baker et al.*, 1996], as this model predicts reconnections between 20 and 30 R_E and only the 28 April 2001 event may be consistent with these large distances. Moreover, to explain the short time delay (~2 min) between reconnection and substorm onset a very high velocity (1000 km s^{-1}) of the plasma flows is required, which is physically possible but unlikely. This short time delay is more consistent with the cross-field current instability model [*Lui*, 1996] where substorms are initiated at shorter distances from the Earth by the disruption of the cross tail current and the formation of a substorm current wedge. The Thermal Catastrophe Model (TCM) [*Goertz and Smith*, 1989] introduced the concept of transfer of energy from the solar wind to the tail plasma to explain the physical role played by the SW pressure pulse. A merging of these models may provide a good representation of the events presented here. This model would include a transfer of energy from the shock to the plasma located in the tail and a modification of the cross tail current at short distances (from 2 R_E for a speed of the plasma flow around 100 km s^{-1} to 7 R_E for a speed of 400 km s^{-1}). These distances are consistent both with the duration of line

Table 1. Integration of the *Liou et al.* [1998] Coupling Function Using ACE Data Measured During the 30 min Preceding the Arrival of the Shock[a]

Date	Type	Integration of the Coupling Function, 10^8 km s^{-1} nT^4
26 Aug 1998	BSINE	7.46
28 Oct 2000	Shock-induced substorm	2.8
27 Nov 2000	Shock-induced substorm	2.07
28 Nov 2000	Shock-induced substorm	7.46
28 Apr 2001	Shock-induced onset	1.5
7 Sep 2002	BSINE	3.03

[a]The 26 August 1998 event was observed by POLAR-UVI and described by *Liou et al.* [1998]; the 7 September 2002 event was observed with IMAGE-FUV.

stretching and the delay between the minimum field line elevation angle and the observed substorm onset.

4.3. Magnetic Perturbation Induced By a Shock

[23] Measurements from GOES satellites show that the arrival of a shock on the front of the magnetosphere is followed by a compression (or dipolarization) of the field in the night region. For two of the three presented events, the enhancement of P_{dyn} last for several hours. During these long-time shocks, GOES observed an important stretching of the tail magnetic field after the compression. The substorm events studied here are observed consecutively to magnetic field dipolarization induced by the shock. These observations are interpreted as a closing of open field lines in the tail due to the Alfvén waves propagation inside the magnetosphere and to the compression of the magnetosphere consecutive to the propagation of the shock along the magnetopause. The stretching of the tail would be consecutive to the viscous interaction of the solar wind with the magnetosphere. A shock can trigger a substorm-like activity if the induced dipolarization occurs when the magnetosphere is unstable. This instability may for example result from a large amount of open flux due to a high rate of dayside reconnection before the shock and to an large enough loading of the magnetosphere allowing the precipitation of the accumulated plasma.

[24] Even though a southward orientation of B_z is commonly accepted as a favorable condition for substorm triggering, the 28 April 2001 event suggests that it is not a necessary condition for the triggering of the onset around midnight. It is interesting to note that shocks occurring during negative B_z conditions may be followed by broad shock-induced nightside enhancements (BSINE) [*Chua et al.*, 2001; *Boudouridis et al.*, 2004; *Milan et al.*, 2004], by substorms, or by no variation of activity in the nightside. Consequently, the ability of a shock to trigger a substorm is not solely dependent on the sign of B_z.

[25] The magnetospheric configuration leading to a substorm expansive phase development induced by a shock rather than to a broad nightside enhancement is still unclear. Mechanisms acting during substorms and BSINE are different since the adiabatic compression and pitch angle diffusion of particles feeding the lost cone play an important role. The state of the magnetosphere is the consequence of the history of the SW-magnetosphere interaction. A good proxy of the energy transfer to the magnetosphere is provided by coupling functions such as discussed by *Liou et al.* [1998]. The integration of the coupling function $VB_t^4 \sin^4(\theta/2)$, where θ is the clock angle which is defined by $\theta = a\cos(B_z/\sqrt{B_y^2 + B_z^2})$, during the 30 min preceding the shock is presented in Table 1.

[26] Values presented in Table 1 do not distinguish the two types of events. However, these values are 10 to 100 times larger than those observed during quiet periods, indicating the need of transfer of a high quantity of energy by SW to the magnetosphere to observe both BSINE and substorm events. The loading appears consequently as a necessary but not as a sufficient condition to observe a substorm induced by a shock.

[27] Particular magnetospheric conditions leading to a substorm rather than to a BSINE when a shock hits the magnetosphere will be addressed in a later study. However, it already appears that the existence of a stretching phase of the tail magnetic field at shock arrival is favorable to substorm triggering. As during the 28 April 2001, this stretching phase may be due to an earlier pressure enhancement. A possible explanation of the relatively rare occurrence of these shock induced event is due to the timescale of magnetospheric loading (tens of minutes to 1 hour or 2). Since this timescale is short with respect to the time between two successive shocks, open flux closure event are mainly due to other causes than magnetospheric perturbation by shocks [*Cowley et al.*, 2005].

5. Conclusion

[28] The question initially addressed by this paper was to examine similarities and differences between nightside shock induced events and classical substorms. We analyzed three events morphologically similar to substorms and beginning within a short time (<20 min) following the arrival of a pressure pulse on the front of the magnetosphere. Different characteristics of these events (mean electron energy, location of the oval before and after onset, power precipitated in the nightside region, and relative proton contribution to the precipitated power) are compared with the classical behavior of substorms. This comparison shows similarities between shock-induced substorms and isolated substorms. Similarities between these two types of events are also present in the dynamic behavior of the magnetic field in the midnight region. It also appears that precipitation observed during onset is due to the dipolarization of the magnetic field induced by the shock rather than to a pitch angle diffusion caused by the curvature of stretched magnetic field lines in the tail. Analysis of the timing of the field line stretching presents similar results to those predicted by the cross-field current instability model. In this context, the role played by the shock is a transfer of energy to the tail plasma and perturbation of the magnetospheric equilibrium which may lead to the reconnection between opposite stretched field lines.

[29] The accumulation of energy from the solar wind in the magnetosphere appears as a necessary condition for the triggering of a substorm by a shock. The release of this energy is initiated by the magnetic field dipolarization

induced by the shock during periods of tail magnetic field stretching for two of the three presented events.

[30] **Acknowledgments.** J.-C. Gérard and B. Hubert are supported by the Belgian Fund for Scientific Research (FNRS), and V. Coumans is supported by a fellowship from the Belgian Fund for Research in Industry and Agriculture (FRIA). The IMAGE-FUV investigation was supported by NASA through SWRI subcontract 83820 at the University of California, Berkeley, contract NAS5-96020. This research was partly funded by the PRODEX program of the European Space Agency. ACE level 2 data were provided by N. F. Ness (MFI) and D. J. McComas (SWEPAM) at the ACE science center through the CDA web. We thank James Weygand and PI R. L. McPherron of UCLA for use of the results of their study "A statistical description of the solar wind at 1 AU and the creation of surrogate time series for input to empirical and numerical models," supported by NASA grant NNG04GA93G. Ground data are used courtesy of the Canadian Space Agency, which constructed and operates the CANOPUS array. Data from the IMAGE magnetometer network are provided by the web site www.ava.fmi.fi/image/request.html.

[31] Arthur Richmond thanks the reviewers for their assistance in evaluating this paper.

References

Akasofu, S. I., and J. K. Chao (1980), Interplanetary shock waves and magnetospheric substorms, *Planet. Space Sci.*, *28*, 381.

Baker, D. N., T. I. Pulkkinen, V. Angelopoulos, W. Baumjohann, and R. L. McPherron (1996), Neutral line model of substorms: Past results and present view, *J. Geophys. Res.*, *101*, 12,975.

Bonnevier, B. R., and G. Rostoker (1970), A three-dimensional model current system for polar magnetic substorms, *J. Geophys. Res.*, *75*, 107.

Boudouridis, A., E. Zesta, L. Lyons, P. Anderson, and D. Lummerzheim (2003), Effect of solar wind pressure pulses on the size and strength of the auroral oval, *J. Geophys. Res.*, *108*(A4), 8012, doi:10.1029/2002JA009373.

Boudouridis, A., E. Zesta, L. R. Lyons, P. C. Anderson, and D. Lummerzheim (2004), Magnetospheric reconnection driven by solar wind pressure fronts, *Ann. Geophys.*, *22*, 1367.

Brittnacher, X., M. Wilber, M. Fillingim, D. Chua, G. Parks, J. Spann, and G. Germany (2000), Global auroral response to a solar wind pressure pulse, *Adv. Space Res.*, *25*, 1377.

Burch, J. L. (1972), Preconditions for the triggering of polar magnetic substorms by storm sudden commencements, *J. Geophys. Res.*, *77*, 5629.

Burch, J. L. (2000), Image mission overview, *Space Sci. Rev.*, *91*, 1–14.

Chua, D., G. Parks, M. Brittnacher, W. Peria, G. Germany, J. Spann, and C. Carlson (2001), Energy characteristics of auroral electron precipitation: A comparison of substorms and pressure pulse related auroral activity, *J. Geophys, Res.*, *106*, 5945.

Coumans, V., J. C. Grard, B. Hubert, and D. S. Evans (2002), Electron and proton excitation of the FUV aurora: Simultaneous IMAGE and NOAA observations, *J. Geophys. Res.*, *107*(A11), 1347, doi:10.1029/2001JA009233.

Coumans, V., J.-C. Grard, B. Hubert, M. Meurant, and S. B. Mende (2004), Global auroral conductance distribution due to electron and proton precipitation from IMAGE-FUV observations, *Ann. Geophys.*, *22*, 1595.

Cowley, S. W. H., S. V. Badman, E. J. Bunce, J. T. Clarke, J.-C. Gérard, D. Grodent, C. M. Jackman, S. E. Milan, and T. K. Yeoman (2005), Reconnection in a rotation-dominated magnetosphere and its relation to Saturn's auroral dynamics, *J. Geophys. Res.*, *110*, A02201, doi:10.1029/2004JA010796.

Cumming, W. D., J. N. Barfield, and P. J. Coleman (1968), Magnetospheric substorms observed at synchronous orbit, *J. Geophys. Res.*, *73*, 6687.

Fairfield, D. H., and N. F. Ness (1970), Configuration of the geomagnetic tail during substorms, *J. Geophys. Res.*, *75*, 7032.

Gérard, J.-C., B. Hubert, M. Meurant, V. I. Shematovich, D. V. Bisikalo, H. Frey, S. B. Mende, G. R. Gladstone, and C. W. Carlson (2001), Observation of proton aurora with IMAGE FUV imager and simultaneous ion flux in situ measurements, *J. Geophys. Res.*, *106*, 939.

Gérard, J.-C., B. Hubert, A. Grard, M. Meurant, and S. B. Mende (2004), Solar wind control of auroral substorm onset locations observed with the image-fuv imagers, *J. Geophys. Res.*, *109*, A03208, doi:10.1029/2003JA010129.

Goertz, C. K., and R. A. Smith (1989), The thermal catastrophe model of substorms, *J. Geophys. Res.*, *94*, 6581.

Hsu, T.-S., and R. L. McPherron (2004), Average characteristics of triggered and nontriggered substorms, *J. Geophys. Res.*, *109*, A07208, doi:10.1029/2003JA009933.

Hubert, B., J. C. Gérard, D. S. Evans, M. Meurant, S. B. Mende, H. U. Frey, and T. J. Immel (2002), Total electron and proton energy input during auroral substorms: Remote sensing with IMAGE-FUV, *J. Geophys. Res.*, *107*(A8), 1183, doi:10.1029/2001JA009229.

Hubert, B., J. C. Gérard, S. A. Fuselier, and S. B. Mende (2003), Observation of dayside subauroral proton flashes with the IMAGE-FUV imagers, *Geophys. Res. Lett.*, *30*(3), 1145, doi:10.1029/2002GL016464.

Hubert, B., J. C. Gérard, S. A. Fuselier, S. B. Mende, and J. L. Burch (2004), Proton precipitation during transpolar auroral events: Observations with the IMAGE-FUV imagers, *J. Geophys. Res.*, *109*, A06204, doi:10.1029/2003JA010136.

Immel, T., J. Craven, and A. Nicholas (2000), An empirical model of the OI FUV dayglow from DE-1 images, *J. Atmos. Sol. Terr. Phys.*, *62*, 47.

Kaufmann, R. L. (1987), Substorm currents: Growth phase and onset, *J. Geophys. Res.*, *92*, 7471.

Kawasaki, K., S.-I. Akasofu, F. Yasuhara, and C.-I. Meng (1971), Storm sudden commencements and polar magnetic substorms, *J. Geophys. Res.*, *76*, 6781.

Kokubun, S., and R. L. McPherron (1981), Substorm signatures at synchronous altitude, *J. Geophys. Res.*, *86*, 11,265.

Kokubun, S., R. L. McPherron, and C. T. Russell (1977), Triggering of substorms by solar wind discontinuities, *J. Geophys. Res.*, *82*, 74.

Kozlovsky, A., V. Safargaleev, N. Østgaard, T. Turunen, A. Koustov, J. Jussila, and A. Roldugin (2005), On the motion of dayside auroras caused by a solar wind pressure pulse, *Ann. Geophys.*, *23*, 509–521.

Liou, K., P. T. Newell, C.-I. Meng, M. Brittnacher, and G. Parks (1998), Characteristics of the solar wind controlled auroral emissions, *J. Geophys. Res.*, *103*, 543.

Liou, K., P. T. Newell, C.-I. Meng, C.-C. Wu, and R. P. Lepping (2002), Do interplanetary shocks really trigger substorm expansion phase onsets?, in *Sixth International Conference on Substorms*, edited by R. M. Winglee, Univ. of Wash., Seattle.

Liou, K., P. T. Newell, C.-I. Meng, C.-C. Wu, and R. Lepping (2003), Investigation of external triggering of substorms with Polar Ultraviolet Imager observation, *J. Geophys. Res.*, *108*(A10), 1364, doi:10.1029/2003JA009984.

Lopez, R. E., D. G. Sibeck, A. T. Y. Lui, K. Takahashi, R. W. McEntire, T. A. Potemra, and D. Klumper (1998), Substorm variations in the magnitude of the magnetic field, *J. Geophys. Res.*, *103*, 14,444.

Lui, A. T. Y. (1996), Current disruption in the earth's magnetosphere: Observations and models, *J. Geophys. Res.*, *101*, 13,067.

Lyons, L. R., G. T. Blanchard, J. C. Samson, R. P. Lepping, T. Yamamoto, and T. Moretto (1997), Coordinated observations demonstrating external substorm triggering, *J. Geophys. Res.*, *102*, 27,039.

McPherron, R. L., C. T. Russell, and M. P. Aubry (1973), Satellite studies of magnetospheric substorms on August 15, 1968: 9. phenomenological model for substorms, *J. Geophys. Res.*, *78*, 3131.

Mende, S. B., H. U. Frey, M. Lampton, J.-C. Gérard, B. Hubert, S. Fuselier, R. Gladstone, and J. L. Burch (2001), Global observations of proton and electron auroras in a substorm, *Geophys. Res. Lett.*, *28*, 1139.

Mende, S. B., H. U. Frey, B. J. Morsony, and T. J. Immel (2003), Statistical behavior of proton and electron auroras during substorms, *J. Geophys. Res.*, *108*(A9), 1339, doi:10.1029/2002JA009751.

Meurant, M., J.-C. Gérard, B. Hubert, C. Blockx, N. Østgaard, and S. Mende (2003a), Dynamics of global scale electron and proton precipitation induced by a solar wind pressure pulse, *Geophys. Res. Lett.*, *30*(20), 2032, doi:10.1029/2003GL018017.

Meurant, M., J.-C. Gérard, B. Hubert, V. Coumans, V. I. Shematovich, D. V. Bisikalo, D. S. Evans, G. R. Gladstone, and S. B. Mende (2003b), Characteristation and dynamics of the auroral precipitation during substorms deduced from IMAGE-FUV, *J. Geophys. Res.*, *108*(A6), 1247, doi:10.1029/2002JA009685.

Meurant, M., J.-C. Gérard, C. Blockx, B. Hubert, and V. Coumans (2004), Propagation of electron and proton shock-induced aurora and the role of the interplanetary magnetic field and solar wind, *J. Geophys. Res.*, *109*, A10210, doi:10.1029/2004JA010453.

Milan, S. E., S. W. H. Cowley, M. Lester, D. M. Wright, J. A. Slavin, M. Fillingim, C. W. Carlson, and H. J. Singer (2004), Response of the magnetotail to changes in the open flux content of the magnetosphere, *J. Geophys. Res.*, *109*, A04220, doi:10.1029/2003JA010350.

Nagai, T. (1982), Observed magnetic substorm signatures at synchronous altitude, *J. Geophys. Res.*, *87*, 4405.

Rostoker, G. (1974), Current flow in the magnetosphere during magnetospheric substorms, *J. Geophys. Res.*, *79*, 1994.

Sauvaud, J.-A., and J. R. Winckler (1980), Dynamics of plasma, energetic particles, and fields near synchronous orbit in the nighttime sector during magnetospheric substorms, *J. Geophys. Res.*, *85*, 2043.

Schieldge, J. P., and G. L. Siscoe (1970), A correlation of the occurrence of simultaneous sudden magnetospheric compression and geomagnetic bay onsets with selected geophysical indices, *J. Atmos. Terr. Phys.*, *32*, 1819.

Tsurutani, B. T., et al. (2001), Auroral zone dayside precipitation during magnetic storm initial phases, *J. Atmos. Sol. Terr. Phys.*, *63*, 513.

Weimer, D. R., D. M. Ober, N. C. Maynard, M. R. Collier, D. J. McComas, N. F. Ness, C. W. Smith, and J. Watermann (2003), Predicting interplanetary magnetic field (IMF) propagation delay times using the minimum variance technique, *J. Geophys. Res.*, *108*(A1), 1026, doi:10.1029/2002JA009405.

Zhou, X.-Y., and B. Tsurutani (1999), Rapid intensification and propagation of the dayside aurora: Large scale interplanetary pressure pulses (fast shocks), *Geophys. Res. Lett.*, *26*, 1097.

Zhou, X.-Y., and B. T. Tsurutani (2001), Interplanetary shock triggering of night-side geomagnetic activity: Substorms, pseudobreakups, and quiescent events, *J. Geophys. Res.*, *106*(18), 957.

Zhou, X.-Y., R. J. Strangeway, P. C. Anderson, D. G. Sibeck, B. T. Tsurutani, G. Haerendel, H. U. Frey, and J. K. Arballo (2003), Shock aurora: FAST and DMSP observations, *J. Geophys. Res.*, *108*(A4), 8019, doi:10.1029/2002JA009701.

C. Blockx, V. Coumans, J.-C. Gérard, B. Hubert, and M. Meurant, Université de Liége, Institut d'Astrophysique et de Geophysique, B5C 17, Allée de 6 Août, 4000 Liége, Belgium. (mmeurant@ulg.ac.be)

M. Connors, Athabasca University, 11560 80 Avenue, Edmonton, T6G OR9, Canada.

E. Donovan, Department of Physics and Astronomy, University of Calgary, 2500 University Drive NW, Calgary, Alberta T2N 1N4, Canada.

L. R. Lyons, Department of Atmospheric Sciences, University of California, Los Angeles, 405 Hilgard Avenue, Los Angeles, CA 90095-1565, USA.